

pubs.acs.org/NanoLett Letter

Ultrathin Free-Standing Oxide Membranes for Electron and Photon Spectroscopy Studies of Solid-Gas and Solid-Liquid Interfaces

Yi-Hsien Lu,[∇] Carlos Morales,[∇] Xiao Zhao,[∇] Matthijs A. van Spronsen, Artem Baskin, David Prendergast, Peidong Yang, Hans A. Bechtel, Edward S. Barnard, D. Frank Ogletree, Virginia Altoe, Leonardo Soriano, Adam M. Schwartzberg, and Miquel Salmeron*



Cite This: https://dx.doi.org/10.1021/acs.nanolett.0c01801



ABSTRACT: Free-standing ultrathin (\sim 2 nm) films of several oxides (Al₂O₃/TiO₂, and others) have been developed, which are mechanically robust and transparent to electrons with $E_{\rm kin} \geq 200$ eV and to photons. We demonstrate their applicability in environmental X-ray photoelectron and infrared spectroscopy for molecular level studies of solid–gas (\geq 1 bar) and solid–liquid interfaces. These films act as membranes closing a reaction cell and as substrates and electrodes for electrochemical reactions. The remarkable properties of such ultrathin oxides membranes enable atomic/molecular level studies of interfacial phenomena, such as corrosion, catalysis, electrochemical reactions, energy storage, geochemistry, and biology, in a broad range of environmental conditions.

KEYWORDS: oxide membranes, electrochemistry, operando spectroscopy, XPS, nano-FTIR

etal and semiconductor oxides are some of the most abundant materials on Earth, and their interactions with aqueous solutions and atmospheric gases are at the base of corrosion, geochemical, catalytic, and electrochemical processes.¹⁻³ In industry, metal-oxides play a crucial role in applications ranging from heterogeneous catalysis, photocatalysis, energy storage, fuel cells, and chemical sensors.⁴⁻⁷ Therefore, the ability to characterize the metal-oxide interface with gases and liquids at the atomic/molecular scale is essential for understanding these processes. Over the past decades, various surface-sensitive techniques have been developed toward this goal. These include electron and X-ray-based spectroscopies, such as X-ray photoelectron spectroscopy (XPS), electron-yield X-ray absorption spectroscopy (EY-XAS), Auger-electron spectroscopy (AES), scanning electron microscopy (SEM), and transmission electron microscopy (TEM), which provide structural and elemental identification of species at surfaces/interfaces. However, the current pressure range where these techniques operate is still lower than that needed in many practical reaction conditions, and their operation in liquid environments remains particularly difficult. To extend the pressure range and to enable measurements in the

liquid phase, thin film membranes acting as windows in environmental cells have been developed recently. Microfabricated thin silicon nitride films (5–200 nm) supported on Si chips are the most popular ones and can be used as window materials for the separation of high vacuum and gases or liquid at ambient pressures. Si, SiO₂, thin carbon films, and graphene have also been used as thin film window materials for this purpose. In particular, graphene has extraordinary mechanical strength and can sustain large pressure differences while being impermeable to gases and liquids. The atomic-scale thickness of graphene makes it sufficiently transparent to electrons and for this reason it has been used in a variety of environmental cells for electron-based microscopies and spectroscopies, such as TEM, SEM, AES, and XPS. 14,17–21 Recently, graphene membranes were also applied in infrared

Received: April 27, 2020 Revised: August 5, 2020 Published: August 5, 2020



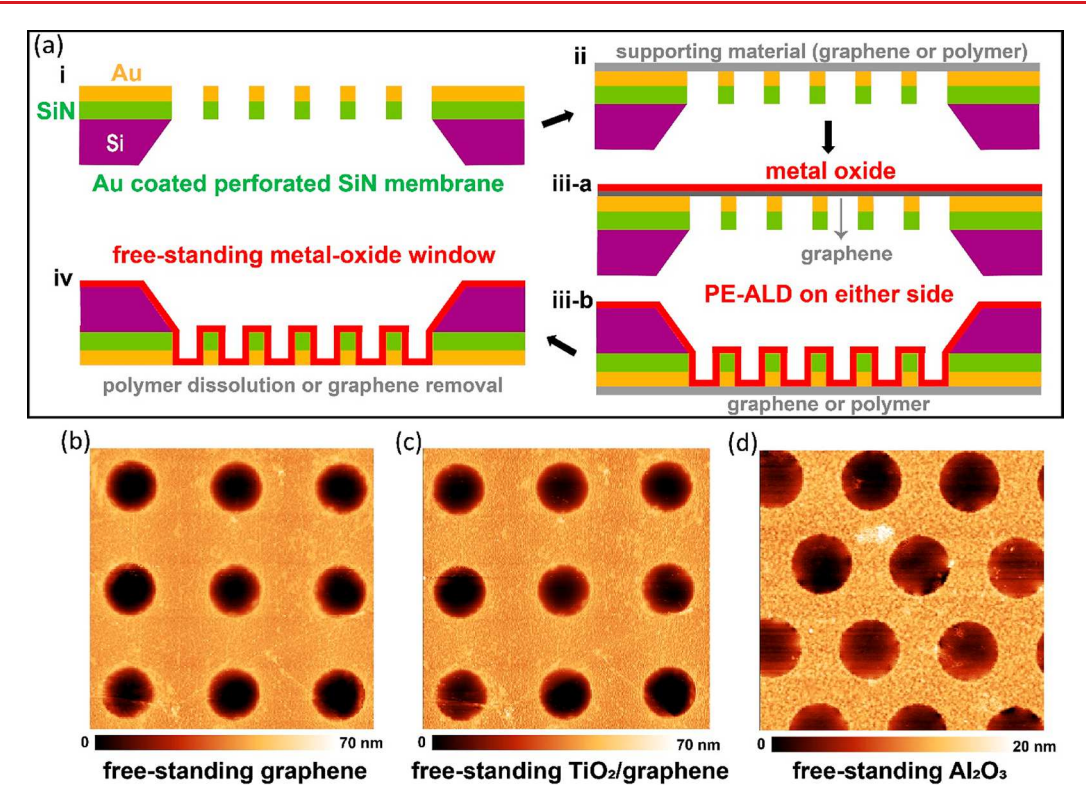


Figure 1. (a) Fabrication process of the free-standing ultrathin metal-oxide membranes. The flat side is exposed to the environment outside the cell, while the corrugated side faces the interior of the cell. (b) AFM topographic image showing a region with a graphene-capped array of holes ($\emptyset = 1 \mu m$), corresponding to step ii. (c) AFM topographic image after deposition of a TiO₂ film (red line in (a)) on the flat side of the graphene showing the uniformity of film (step iii-a). (d) AFM topographic image showing a region with a 2-nm-thick Al₂O₃ film covering the holes ($\emptyset = 500$ nm, step (iv)). In this case, Formvar polymer was used as a support for the PE-ALD process on the corrugated side and dissolved afterward, leaving the Al₂O₃ film suspended.

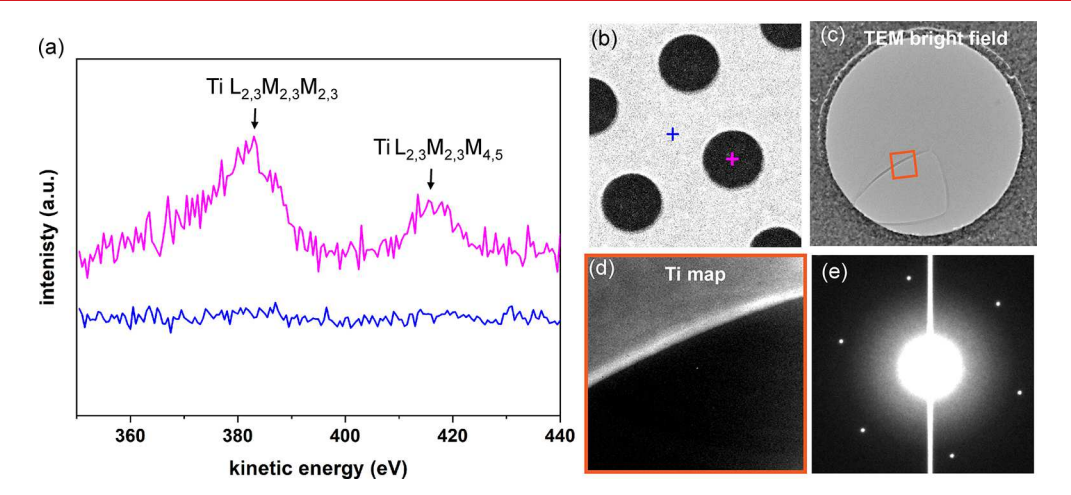


Figure 2. (a) High spatial resolution (a few nm) Auger-electron spectroscopy on the graphene/Au/SiN region (blue) and on the free-standing graphene/TiO₂ window (magenta). Electron beam was illuminated from the side opposite to the TiO_2 deposition. (b) SEM image showing marks at the location where the Auger spectra were taken. (c) TEM bright-field image from a partially ruptured graphene/TiO₂ window (\emptyset = 1000 nm). (d) EELS (Ti-L edge) map from the region marked by a square in (c) containing the edge of the ruptured. (e) Electron diffraction pattern from a TiO_2 / graphene region showing the hexagonal pattern from graphene with the amorphous TiO_2 contributing only to the background.

(IR) nanospectroscopy (nano-FTIR) studies of the molecular structure of liquids near graphene.²²

Here we present a new generation of ultrathin (few nm) membranes based on oxide materials. These ultrathin oxides have remarkable mechanical strength and can withstand large pressure differences (≥1 bar), which makes them useful as cell membrane windows. Like graphene, as we will show, they are transparent to photons and to electrons with a wide range of

kinetic energies. The membranes can be used as supports of

metal particles for catalysis studies, as electrodes in electro-

catalysis, in batteries, and in many other applications.

■ FABRICATION AND CHEMICAL COMPOSITION OF THE METAL-OXIDE FILMS

Figure 1a shows a schematic representation of the fabrication process. We start with commercial silicon nitride membranes, abbreviated as SiN, perforated with holes of 500-2000 nm diameter. We coat these membranes with gold (or other metals), Figure 1a step i, and subsequently cover them with a graphene layer on the flat side (Figure 1a step ii). The purpose of gold is to improve adhesion and to ensure good electrical connectivity between graphene domains. The oxide film is grown by plasmaenhanced atomic layer deposition (PE-ALD)²³⁻²⁷ on either side of the graphene, 23-25 as illustrated in Figure 1a step iii-a and iiib. The graphene can be removed, if desired, by oxygen plasma to leave only the suspended metal-oxide (step iv in Figure 1a). Typically, however, we keep the graphene on the external side of the window as it adds mechanical strength and because it provides good electrical conductivity for biasing the metal-oxide when acting as an electrode. Figure 1b shows an atomic-force microscopy (AFM) topographic image of a region of the SiN sample with holes capped with graphene, while Figure 1c is an image of the same area with a 2-nm-thick TiO2 film grown on the flat side, showing its excellent conformal distribution. Figure 1d shows a region of an Al₂O₃-covered array of holes, which were initially covered by a Formvar polymer (polyvinyl formal). The polymer acts as support for the PE-ALD growth and was subsequently dissolved in chloroform so that the metal-oxide membrane is freely suspended. The details about the PE-ALD growth and the transfer process can be found in the Supporting Information. The local thickness of the metal-oxides was estimated by electron energy-loss spectroscopy (EELS) using the log-ratio method (Figure S2).²⁸ Other measurements using AFM and ellipsometry are described in the Supporting Information.

The chemical composition and uniformity of the films were examined by scanning Auger-electron spectroscopy (with a spatial resolution of a few nm) and by TEM/EELS. As shown in Figure 2a, when TiO₂ is deposited on the side facing the cell interior (corresponding to the SEM image in Figure 2b), the Ti LMM Auger-electron peaks only appear when the electron beam is focused on the free-standing graphene/TiO2 (magenta) but not on the region between holes (blue). Because of the short inelastic mean free path of the 380 eV Auger electrons (around 1 nm), the spectra show only Ti peaks on the suspended graphene region of the membrane. Figure 2c shows a TEM image of a region of a SiN sample with a hole partly covered by a freestanding graphene/TiO₂ membrane (the missing part of the membrane is the brightest part). Figure 2d shows a map of the Ti-L_{2,3} loss peak intensity (EELS) from the region marked by a square in Figure 2c that includes the ruptured edge. The smoothness of the contrast over the film, and its abrupt change across the edge, demonstrates the chemical uniformity of the metal-oxide layer over the free-standing graphene. An electrondiffraction pattern from the graphene/TiO2 area is shown in Figure 2e. Only the hexagonal diffraction pattern can be seen and it must be from graphene since at this low-temperature (40-120 °C) PE-ALD conditions, the metal-oxide is expected to be amorphous and does not produce diffracted beams. 23-26,29 Similar results were obtained for Al₂O₃/graphene membranes (Figure S3).

At the temperature used in the PE-ALD growth process, a high content of carbon (around 15%) was observed by XPS as a residue of the organic precursor. Surface OH⁻ groups could also

bring out an excess of oxygen. 30,31 In a separate test, a 20-nm-thick $\mathrm{Al_2O_3}$ layer was grown on a SiN wafer to study in more detail its chemical composition and the possibility of cleaning the surface $\mathrm{OH^-}$ groups without altering the structural quality of the ultrathin membranes. Figure S4 shows an XPS depth-profile measurement and how the initial element concentrations of the uppermost layer converge to the stoichiometric 3/2:O/Al ratio in the bulk. The profile also shows that the carbon content drops to less than 2% in the $\mathrm{Al_2O_3}$ bulk. The carbon and $\mathrm{OH^-}$ groups can be eliminated by a gentle sputtering with $\mathrm{Ar_{75}^+}$ clusters at 8000 eV without discernible damage on the ultrathin film (Table S1). 32

MECHANICAL PROPERTIES OF METAL-OXIDE FILMS

The mechanical behavior of the free-standing metal-oxide membranes was investigated by nanoindentation using an AFM tip. To rule out indentation-induced damage to the tip, AFM topographic images were acquired before and after each indentation. Figure 3 shows representative force—distance

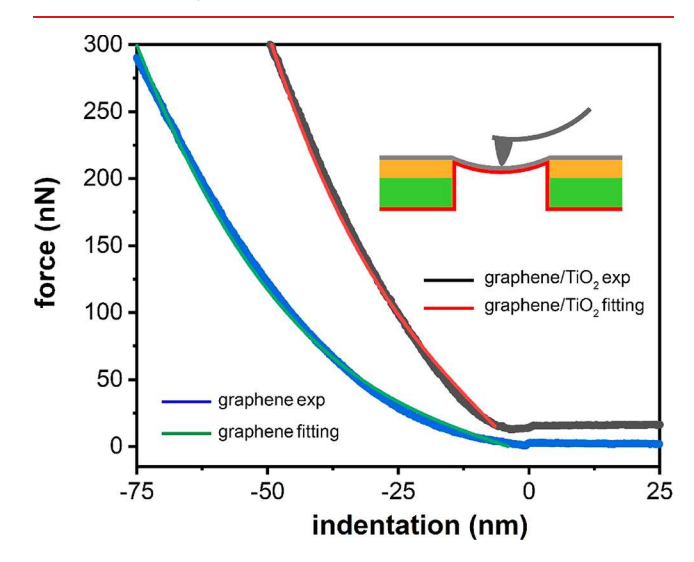


Figure 3. AFM nanoindentation curves of suspended graphene (blue) and graphene/ TiO_2 (black). The green and red curves correspond to the fitting results of graphene and graphene/ TiO_2 , respectively, using eq 1. The inset shows a schematic of the AFM nanoindentation experiment.

curves on a 1- μ m-diameter hole covered with a suspended graphene membrane without (blue) and with (black) a 2-nm-thick TiO₂ film deposited on the side facing the cell interior. Details of the AFM nanoindentation can be found in Methods. Only a small difference is visible between the loading and unloading curves in both cases, suggesting an elastic deformation process and no sliding between the graphene and TiO₂ layers during indentation, indicative of strong adhesion between graphene and TiO₂. The effective Young's modulus (*E*) of the suspended membrane was calculated using eq 1, 15,24,25 which describes the force versus indentation depth of a suspended clamped circular sheet of an isotropic elastic material under a centrally applied load

$$F = \left[3 \frac{4\pi E}{1 - \nu^2} \left(\frac{t^3}{a^2} \right) \right] \delta + (\pi T) \delta + \left(\frac{q^3 E t}{a^2} \right) \delta^3$$
 (1)

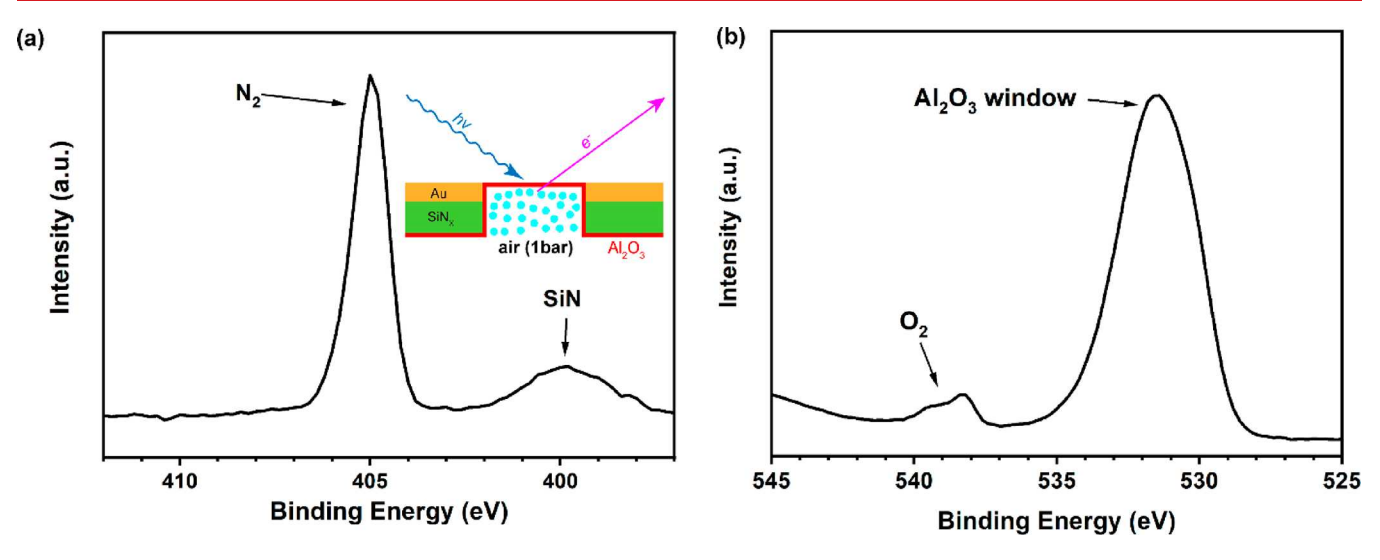


Figure 4. XPS measurements through a 2-nm-thick Al_2O_3 membrane closing a cell filled with 1 bar of air. The cell is located inside an XPS vacuum chamber with a 10^{-6} to 10^{-7} -Torr base pressure. (a) N 1s spectrum containing a sharp peak from $N_2(g)$ in air and a smaller peak from the SiN support. (b) O 1s spectrum showing the doublet peak from $O_2(g)$ in air and a strong, broad peak from Al_2O_3 . The photon energy is 1135 eV.

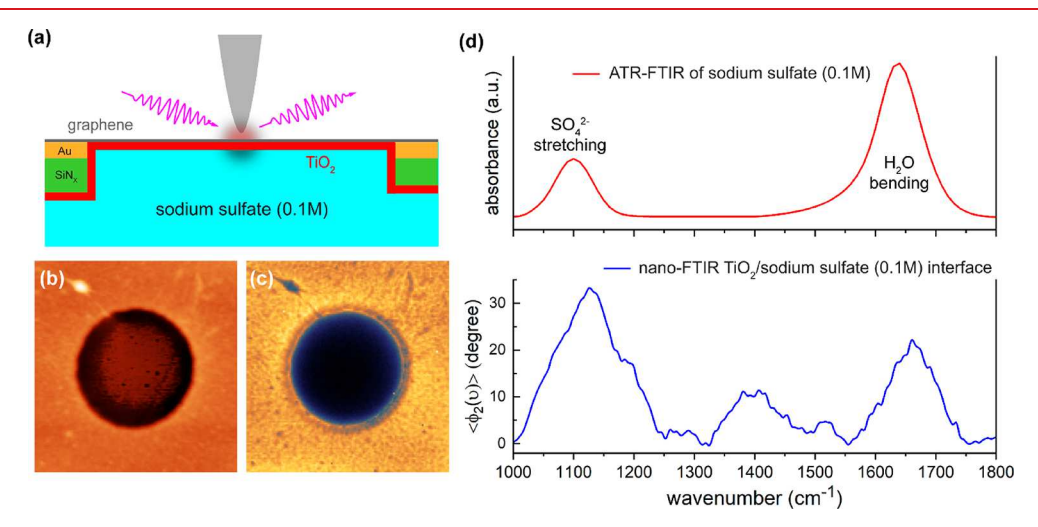


Figure 5. (a) Schematic of the plasmonically enhanced nano-FTIR experiment with the AFM tip situated over the metal-oxide window closing the cell filled with liquid. Broadband synchrotron IR radiation is focused on the apex of the AFM tip, which enhances the electromagnetic field in the proximity of the apex in a range roughly equal to the tip radius (few nm) and scatters it to the far field. (b) Topography and (c) second-harmonic optical amplitude images from the IR light scattered by the tip over the graphene/ TiO_2 window covering a sodium sulfate aqueous solution (0.1 M) inside the cell. (d) Top: ATR-FTIR from a droplet of 0.1 M sodium sulfate aqueous solution. Bottom: nano-FTIR of the 0.1 M sodium sulfate solution acquired with the tip over the graphene/ TiO_2 window (3 nm thick). The nano-FTIR spectrum is obtained from the phase of the scattered signal at the second harmonic of the cantilever oscillation frequency, which corresponds to the absorption coefficient of the material. A2,43,47 Notice the different amplitudes of the bulk (ATR-FTIR) and nano-FTIR peaks of the SO_4^{2-} -stretching and water-bending modes, and the presence of additional peaks between these two, visible only in the near-surface region detected by nano-FTIR, showing the difference in composition between the bulk and the near-surface region (nm).

where t = thickness of the suspended membrane, ν = effective Poisson's ratio, a = radius of the suspended membrane, T = pretension in the suspended membrane, q is a dimensionless parameter equal to $1/(1.05-0.15\nu-0.16\nu^2)$, F = applied force, and δ = indentation depth. By using eq 1 and fitting the force—indentation curves, shown in Figure 3 as green and red curves corresponding to graphene and graphene/TiO₂, respectively, we obtain the Young's modulus of graphene, $E_{\rm graphene}$, of around 404 \pm 14 GPa and that of the 2-nm-thick TiO₂ film on graphene, $E_{\rm graphene/TiO2}$ of 200 \pm 100 GPa. These values are close to the values reported in the literature. The $E_{\rm graphene}$ value, however, is lower than that reported for graphene prepared by mechanical exfoliation of graphite (\sim 1 TPa), which could be due to defects in the graphene used in this study stemming from

the chemical-vapor-deposition process and/or from the transfer processes. Assuming a tip radius between 10 and 50 nm, we estimate that our free-standing metal-oxide membrane can withstand pressures higher than 10^6 Pa, that is, more than 10 bar, which explains its good performance as an environmental-cell window to contain high-pressure gas or liquids.

METAL-OXIDE MEMBRANES FOR ELECTRON SPECTROSCOPY STUDIES OF SOLID—GAS INTERFACES

The submicrometer thickness of SiN membranes (and other materials) makes them transparent to high-energy radiation, in particular $\geq \! 100$ keV electrons and X-rays, and for that reason

they are frequently used for TEM9,33 and X-rays absorption spectroscopies in fluorescent-yield detection mode (FY-XAS) 34,35 Surface sensitive spectroscopies such as XPS and EY-XAS, which use emitted electrons traversing the membrane, are not possible with standard SiN membranes because of the short mean free path of a few nanometers of low-energy electrons in solid materials. However, the ultrathin metal-oxide films presented above make possible XPS measurements of species present near the membrane, similar to the case of graphene. 21 Figure 4a,b shows the N 1s and O 1s photoelectron spectra from air at 1 bar enclosed by a 2-nm-thick Al₂O₃ freestanding membrane. The cell is located inside a vacuum chamber with 10^{-6} – 10^{-7} -Torr base pressure containing an XPS spectrometer. In Figure 4a, The N 1s spectrum shows a sharp peak at a binding energy of ~405 eV from the N₂ gas phase, together with a small contribution at ~400 eV from N in the SiN support.²¹ Similarly, in Figure 4b the O 1s spectrum shows a doublet peak (due to paramagnetic splitting) at ~537-540 eV corresponding to the O₂ gas phase 36,37 and another peak at 532.5 eV from the O in the Al₂O₃ membrane. The integrated intensity ratio of the N2 to O2 peaks is close to 4, as expected from the air composition.

■ INFRARED SPECTROSCOPY STUDIES AT THE INTERFACE BETWEEN METAL-OXIDE AND LIQUID

Vibrational spectroscopies based on photons, such as Fouriertransform infrared spectroscopy (FTIR), Raman spectroscopy, and sum-frequency-generation spectroscopy (SFG) are powerful and noninvasive tools for studies of surfaces and interfaces.³⁸⁻⁴¹ Most materials, especially insulating metaloxides, are highly transparent to visible and infrared light, and thus they allow for easy access to the buried solid-liquid interface. The lack of spatial resolution, particularly in the IR case, can be overcome by taking advantage of the plasmonic enhancement in confined geometries and near the corners of sharp objects. 42-44 We recently demonstrated this using an AFM tip to achieve nanoscale resolution FTIR spectra through a graphene membrane electrode to determine the nature of the species in the vicinity of the electrode (i.e., in the electrical double layer) and their variation with applied bias. 22 Here, we demonstrate that this is also possible with our ultrathin graphene/metal-oxide membranes. Figure 5a shows the schematic of the nano-FTIR measurement through the graphene/TiO2 window of a liquid in the cell. Figure 5b is the AFM topographic image of a region containing a graphene/ TiO₂ (3 nm thick) window in contact with a 0.1 M sodium sulfate aqueous solution. The corresponding amplitude of the scattered IR light at the second harmonic of the tip oscillation is shown in Figure 5c. The amplitude over the graphene/TiO₂ window (dark color) is much smaller than that over the graphene-gold region (gold color), as expected from the negligible absorption of graphene/gold compared to the poorly reflective graphene/TiO2 window. The nano-FTIR spectrum of a 0.1 M sodium sulfate solution in contact with the TiO2 of the graphene/TiO2 membrane at open circuit condition (averaged from spectra acquired on many points in the membrane) is shown at the bottom of Figure 5d. For comparison, the attenuated total reflection FTIR (ATR-FTIR) from a 0.1 M droplet of aqueous sodium sulfate solution is shown at the top in Figure 5d. As can be seen, the expected peaks from the antisymmetric S=O stretching mode in SO_4^{2-} (around 1100 cm⁻¹) and from the bending mode of water (~1650 cm⁻¹) are visible in both cases. However, the sulfate-to-water-peak ratio in

nano-FTIR is much larger than that of the ATR-FTIR measurements with the former reflecting the near-surface region (nm) while the latter reflects the bulk (μ m) composition of the solution. Several additional peaks between 1200 and 1600 cm⁻¹ are also present in the nano-FTIR spetrum, the nature of which is still under investigation. Interestingly, while in the case of a pure graphene membrane in contact with 0.1 M ammonium sulfate solution, the sulfate peak is about 4 times more intense than that of water, the ratio near the TiO₂ film is about 2 or less. These results indicate that the structure of the electrolyte in the electrical double layer is highly influenced by the nature of the electrode and by the additional hydrogenbonding of water with O in the metal-oxide surface, which provides an anchoring and orienting mechanism for water that is very different from that in the hydrophobic graphene.

In summary, we have shown that mechanically robust, freestanding, ultrathin metal-oxide membranes can be fabricated by PE-ALD on graphene and on polymer supports. The oxide membranes are amorphous, uniform in thickness, and have compositions similar to those of the corresponding bulk oxides. Our proof-of-concept experiments show that they can be used as windows in environmental cells for XPS and nano-FTIR spectroscopic studies of gases (>1 bar) and of liquids near the interface. Their small thickness and good mechanical strength make them applicable to other electron/X-ray microscopy/ spectroscopy or scanning probe techniques. By using different precursors and growing temperatures, a wide range of oxides of metals and semiconductors, including SiO₂, CoO_x, HfO₂, and so forth, could be fabricated and used as suspended ultrathin films with different stoichiometry and crystallinity. 26,29,48 Therefore, we anticipate that the platform developed and presented here will open up new avenues for the study of catalytic, electrochemical, geochemical, and other reactions at interfaces in practical conditions, as demonstrated by the results reported here. In addition, the ALD technique can also be used to grow membranes of other practical materials, such as nitrides, sulfides, noble metals, and 2D materials. 26,29,48,49 Besides the applications for chemical studies just mentioned, the physical properties of the ultrathin metal-oxides can vary substantially from those of their bulk counterparts, including their magnetic properties and electron conductivity, which will be explored in the future. In the device area, the subsequent deposition of periodic array structures with different dielectric constants could be an ideal platform for photonic crystals and may be useful for vibrational spectroscopies and biochemical sensors.⁵

METHODS

Characterization of Metal-Oxide Thin Films. The characterization of the metal-oxides films was performed by XPS, TEM, scanning Auger-electron spectroscopy, and AFM measurements. The XPS measurements were performed using K-Alpha Plus XPS/UPS analyzer from Thermo Fisher Scientific equipped with a monochromatic Al K_{α} X-ray source (1486.6 eV) and an ion gun (Ar⁺ or Ar₇₅⁺) in an ultrahigh vacuum chamber. A flood gun was used during the measurements. TEM and EELS measurements were performed with a JEOL 2100-F 200 kV field-emission analytical TEM at an electron energy of 200-kV. Scanning Auger-electron spectroscopy measurements were performed with an Oxford/Omicron Nano-Auger system under ultrahigh vacuum of 10⁻¹⁰ Torr. The size of the electron-beam spot was ~10 nm. AFM topography measurements were done using Cypher ES (Asylum Research) and Bruker Icon systems.

AFM Nanoindentation. The AFM nanoindentation was performed using the Cypher ES (Asylum Research). The normal spring constant of the cantilever was calibrated using the Sader Method. The indentation rate was around 0.2 μ m s⁻¹. A topographic scan was acquired before the indentation, and the tip was positioned at the center of the suspended membrane for indentation measurements.

In Situ XPS and Nano-FTIR Measurements. In situ XPS measurements were performed using the APPES-II end station in beamline 11.0.2 of the Advanced Light Source, at the Lawrence Berkeley National Laboratory. A differentially pumped analyzer (Phoibos 150, SPECS GmbH) equipped with three differentially pumped electrostatic lenses was used. The design of the gas cell can be found elsewhere. ²¹

Nano-FTIR measurements were performed at beamline 2.4 of the Advanced Light Source, at the Lawrence Berkeley National Laboratory. The infrared light was focused onto the apex of a Ptcoated AFM tip in a neaSNOM (Neaspec, Germany) system. Tapping-mode operation was performed at the fundamental resonance frequency of the cantilever (250-350 kHz) with a free oscillation amplitude ranging from 70 to 90 nm and an amplitude setpoint of ~80%. The scattered near-field signal is retrieved by a lock-in amplifier tuned to the second and higher harmonics of the cantilever oscillation to eliminate the far-field nonlocal scattered background. The complex-valued near-field spectrum is derived from a Fourier transform of the interferogram. The Fourier components are presented as real spectral amplitude "A" and phase " ϕ ", normalized to reference spectra: $A_i(v) = A_i^{\text{sample}}(v)/A_i^{\text{reference}}(v)$ and $\phi_i(v) = \phi_i^{\text{sample}}(v)$ - $\phi_i^{\text{reference}}(v)$ where v is the wavenumber. Reference spectra were taken on samples with flat spectral responses, either Aucoated Si or graphene on the Au-coated SiN membrane. The phase ϕ contains the absorption coefficient of materials and has been shown to be in good agreement with traditional FTIR absorption measurements. 42,43,4

■ ASSOCIATED CONTENT

Supporting Information

The Supporting Information is available free of charge at https://pubs.acs.org/doi/10.1021/acs.nanolett.0c01801.

PE-ALD growth of metal-oxides, graphene and polymer transfer on perforated SiN membranes, thickness estimation of free-standing metal-oxides by EELS, TEM/EELS characterization of free-standing ${\rm Al}_2{\rm O}_3$ windows, and XPS depth profile analysis of ${\rm Al}_2{\rm O}_3$ thin film (PDF)

AUTHOR INFORMATION

Corresponding Author

Miquel Salmeron — Materials Sciences Division, Lawrence Berkeley National Laboratory, Berkeley, California 94720, United States; Department of Materials Science and Engineering, University of California at Berkeley, Berkeley, California 94720, United States; orcid.org/0000-0002-2887-8128; Email: mbsalmeron@lbl.gov

Authors

Yi-Hsien Lu — Materials Sciences Division, Lawrence Berkeley National Laboratory, Berkeley, California 94720, United States; orcid.org/0000-0001-6572-5553

Carlos Morales — Materials Sciences Division, Lawrence Berkeley National Laboratory, Berkeley, California 94720, United States; Departamento de Fisica Aplicada and Instituto de Ciencia de Materiales Nicolás Cabrera, Universidad Autónoma de Madrid, 28049 Madrid, Spain; o orcid.org/0000-0001-5890-1950

Xiao Zhao — Materials Sciences Division, Lawrence Berkeley National Laboratory, Berkeley, California 94720, United States; Department of Materials Science and Engineering, University of California at Berkeley, Berkeley, California 94720, United States; orcid.org/0000-0003-1079-664X

Matthijs A. van Spronsen − Materials Sciences Division, Lawrence Berkeley National Laboratory, Berkeley, California 94720, United States; orcid.org/0000-0002-5136-2816

Artem Baskin — Molecular Foundry, Lawrence Berkeley National Laboratory, Berkeley, California 94720, United States;
orcid.org/0000-0002-3156-6256

David Prendergast — Molecular Foundry, Lawrence Berkeley National Laboratory, Berkeley, California 94720, United States Peidong Yang — Materials Sciences Division, Lawrence Berkeley National Laboratory, Berkeley, California 94720, United States; Department of Chemistry, University of California, Berkeley, California 94720, United States; orcid.org/0000-0003-4799-1684

Hans A. Bechtel — Advanced Light Source, Lawrence Berkeley
National Laboratory, Berkeley, California 94720, United States
Edward S. Barnard — Molecular Foundry, Lawrence Berkeley
National Laboratory, Berkeley, California 94720, United States
D. Frank Ogletree — Molecular Foundry, Lawrence Berkeley
National Laboratory, Berkeley, California 94720, United States
Virginia Altoe — Molecular Foundry, Lawrence Berkeley National
Laboratory, Berkeley, California 94720, United States
Leonardo Soriano — Departamento de Fisica Aplicada and
Instituto de Ciencia de Materiales Nicolás Cabrera, Universidad

Autónoma de Madrid, 28049 Madrid, Spain; orcid.org/ 0000-0001-5715-376X Adam M. Schwartzberg — Molecular Foundry, Lawrence Berkeley National Laboratory, Berkeley, California 94720,

United States; © orcid.org/0000-0001-6335-0719

Complete contact information is available at: https://pubs.acs.org/10.1021/acs.nanolett.0c01801

Author Contributions

Y.-H.L., C.M., and X.Z. contributed equally to this work.

The authors declare no competing financial interest.

■ ACKNOWLEDGMENTS

We are grateful to Ed Wong of the Molecular Foundry for assistance in fabricating the gas cell. This work was supported by the Office of Basic Energy Sciences (BES), Division of Materials Sciences and Engineering, of the U.S. Department of Energy (DOE) under Contract DE-AC02-05CH11231, through the Structure and Dynamics of Materials Interfaces program (FWP KC31SM). Work was performed at the Molecular Foundry and at the Advanced Light Source user facilities, supported by the DOE Office of Basic Energy Sciences under the same contract number. X.Z was supported by a NSF-BSF grant number 1906014. C.M thanks the MEDC for a FPU fellowship grant (FPU14/02020).

REFERENCES

(1) Putnis, C. V.; Ruiz-Agudo, E. The Mineral-Water Interface: Where Minerals React with the Environment. *Elements* **2013**, *9* (3), 177–182.

- (2) Brown, G. E.; Henrich, V. E.; Casey, W. H.; Clark, D. L.; Eggleston, C.; Felmy, A.; Goodman, D. W.; Gratzel, M.; Maciel, G.; McCarthy, M. I.; Nealson, K. H.; Sverjensky, D. A.; Toney, M. F.; Zachara, J. M. Metal oxide surfaces and their interactions with aqueous solutions and microbial organisms. *Chem. Rev.* **1999**, *99* (1), 77–174.
- (3) Al-Abadleh, H. A.; Grassian, V. H. Oxide surfaces as environmental interfaces. *Surf. Sci. Rep.* **2003**, *52* (3–4), 63–161.
- (4) Zhao, Y.; Li, X. F.; Yan, B.; Xiong, D. B.; Li, D. J.; Lawes, S.; Sun, X. L. Recent Developments and Understanding of Novel Mixed Transition-Metal Oxides as Anodes in Lithium Ion Batteries. *Adv. Energy Mater.* **2016**, *6* (8), 1502175.
- (5) Wu, Y. Metal oxides in energy technologies, 1st ed.; Elsevier: London, 2018.
- (6) Dey, A. Semiconductor metal oxide gas sensors: A review. *Mater. Sci. Eng., B* **2018**, 229, 206–217.
- (7) Jackson, S. D.; Hargreaves, J. S. J. Metal oxide catalysis; Wiley-VCH: Weinheim, 2008.
- (8) Somorjai, G. A.; Li, Y. Introduction to surface chemistry and catalysis, 2nd ed.; Wiley: Hoboken, NJ, 2010.
- (9) de Jonge, N.; Ross, F. M. Electron microscopy of specimens in liquid. *Nat. Nanotechnol.* **2011**, *6* (11), 695–704.
- (10) Velasco-Velez, J. J.; Wu, C. H.; Pascal, T. A.; Wan, L. W. F.; Guo, J. H.; Prendergast, D.; Salmeron, M. The structure of interfacial water on gold electrodes studied by x-ray absorption spectroscopy. *Science* **2014**, *346* (6211), 831–834.
- (11) Hatty, V.; Kahn, H.; Heuer, A. H. Fracture toughness, fracture strength, and stress corrosion cracking of silicon dioxide thin films. *J. Microelectromech. Syst.* **2008**, *17* (4), 943–947.
- (12) Striemer, C. C.; Gaborski, T. R.; McGrath, J. L.; Fauchet, P. M. Charge- and size-based separation of macromolecules using ultrathin silicon membranes. *Nature* **2007**, *445* (7129), 749–753.
- (13) Daulton, T. L.; Little, B. J.; Lowe, K.; Jones-Meehan, J. In situ environmental cell-transmission electron microscopy study of microbial reduction of chromium(VI) using electron energy loss spectroscopy. *Microsc. Microanal.* **2001**, *7* (6), 470–485.
- (14) Yuk, J. M.; Park, J.; Ercius, P.; Kim, K.; Hellebusch, D. J.; Crommie, M. F.; Lee, J. Y.; Zettl, A.; Alivisatos, A. P. High-Resolution EM of Colloidal Nanocrystal Growth Using Graphene Liquid Cells. *Science* **2012**, 336 (6077), 61–64.
- (15) Lee, C.; Wei, X. D.; Kysar, J. W.; Hone, J. Measurement of the elastic properties and intrinsic strength of monolayer graphene. *Science* **2008**, 321 (5887), 385–388.
- (16) Bunch, J. S.; Verbridge, S. S.; Alden, J. S.; van der Zande, A. M.; Parpia, J. M.; Craighead, H. G.; McEuen, P. L. Impermeable atomic membranes from graphene sheets. *Nano Lett.* **2008**, 8 (8), 2458–2462.
- (17) Yulaev, A.; Guo, H. X.; Strelcov, E.; Chen, L.; Vlassiouk, I.; Kolmakov, A. Graphene Microcapsule Arrays for Combinatorial Electron Microscopy and Spectroscopy in Liquids. *ACS Appl. Mater. Interfaces* **2017**, 9 (31), 26492–26502.
- (18) Kolmakov, A.; Dikin, D. A.; Cote, L. J.; Huang, J. X.; Abyaneh, M. K.; Amati, M.; Gregoratti, L.; Gunther, S.; Kiskinova, M. Graphene oxide windows for in situ environmental cell photoelectron spectroscopy. *Nat. Nanotechnol.* **2011**, *6* (10), 651–657.
- (19) Velasco-Velez, J. J.; Pfeifer, V.; Havecker, M.; Weatherup, R. S.; Arrigo, R.; Chuang, C. H.; Stotz, E.; Weinberg, G.; Salmeron, M.; Schlögl, R.; Knop-Gericke, A. Photoelectron Spectroscopy at the Graphene-Liquid Interface Reveals the Electronic Structure of an Electrodeposited Cobalt/Graphene Electrocatalyst. *Angew. Chem., Int. Ed.* 2015, 54 (48), 14554–14558.
- (20) Guo, H. X.; Strelcov, E.; Yulaev, A.; Wang, J.; Appathurai, N.; Urquhart, S.; Vinson, J.; Sahu, S.; Zwolak, M.; Kolmakov, A. Enabling Photoemission Electron Microscopy in Liquids via Graphene-Capped Microchannel Arrays. *Nano Lett.* **2017**, *17* (2), 1034–1041.
- (21) Weatherup, R. S.; Eren, B.; Hao, Y. B.; Bluhm, H.; Salmeron, M. B. Graphene Membranes for Atmospheric Pressure Photoelectron Spectroscopy. *J. Phys. Chem. Lett.* **2016**, 7 (9), 1622–1627.
- (22) Lu, Y. H.; Larson, J. M.; Baskin, A.; Zhao, X.; Ashby, P. D.; Prendergast, D.; Bechtel, H. A.; Kostecki, R.; Salmeron, M. Infrared

- Nanospectroscopy at the Graphene-Electrolyte Interface. *Nano Lett.* **2019**, *19* (8), 5388–5393.
- (23) Wang, L. D.; Travis, J. J.; Cavanagh, A. S.; Liu, X. H.; Koenig, S. P.; Huang, P. Y.; George, S. M.; Bunch, J. S. Ultrathin Oxide Films by Atomic Layer Deposition on Graphene. *Nano Lett.* **2012**, *12* (7), 3706–3710.
- (24) Cao, C. H.; Mukherjee, S.; Liu, J.; Wang, B. Q.; Amirmaleki, M.; Lu, Z. L.; Howe, J. Y.; Perovic, D.; Sun, X. L.; Singh, C. V.; Sun, Y.; Filleter, T. Role of graphene in enhancing the mechanical properties of TiO2/graphene heterostructures. *Nanoscale* **2017**, *9* (32), 11678–11684
- (25) Munther, M.; Shaygan, M.; Centeno, A.; Neumaier, D.; Zurutuza, A.; Momeni, K.; Davami, K. Probing the mechanical properties of vertically-stacked ultrathin graphene/Al2O3 heterostructures. *Nanotechnology* **2019**, *30* (18), 185703.
- (26) George, S. M. Atomic Layer Deposition: An Overview. Chem. Rev. 2010, 110 (1), 111-131.
- (27) Singh, S.; Mahalingam, H.; Singh, P. K. Polymer-supported titanium dioxide photocatalysts for environmental remediation: A review. *Appl. Catal., A* **2013**, *462*, 178–195.
- (28) Egerton, R. F. Electron energy-loss spectroscopy in the electron microscope, 3rd ed.; Springer: New York, 2011.
- (29) Profijt, H. B.; Potts, S. E.; van de Sanden, M. C. M.; Kessels, W. M. M. Plasma-Assisted Atomic Layer Deposition: Basics, Opportunities, and Challenges. *J. Vac. Sci. Technol.*, A 2011, 29 (5), 050801.
- (30) Gosset, L. G.; Damlencourt, J. F.; Renault, O.; Rouchon, D.; Holliger, P.; Ermolieff, A.; Trimaille, I.; Ganem, J. J.; Martin, F.; Semeria, M. N. Interface and material characterization of thin Al₂O₃ layers deposited by ALD using TMA/H₂O. *J. Non-Cryst. Solids* **2002**, 303 (1), 17–23.
- (31) Haeberle, J.; Henkel, K.; Gargouri, H.; Naumann, F.; Gruska, B.; Arens, M.; Tallarida, M.; Schmeisser, D. Ellipsometry and XPS comparative studies of thermal and plasma enhanced atomic layer deposited Al₂O₃-films. *Beilstein J. Nanotechnol.* **2013**, *4*, 732–742.
- (32) Simpson, R.; White, R. G.; Watts, J. F.; Baker, M. A. XPS investigation of monatomic and cluster argon ion sputtering of tantalum pentoxide. *Appl. Surf. Sci.* **2017**, 405, 79–87.
- (33) Ring, E. A.; Peckys, D. B.; Dukes, M. J.; Baudoin, J. P.; de Jonge, N. Silicon nitride windows for electron microscopy of whole cells. *J. Microsc.* **2011**, 243 (3), 273–283.
- (34) Guo, J. H.; Luo, Y.; Augustsson, A.; Rubensson, J. E.; Sathe, C.; Agren, H.; Siegbahn, H.; Nordgren, J. X-ray emission spectroscopy of hydrogen bonding and electronic structure of liquid water. *Phys. Rev. Lett.* **2002**, 89 (13), 137402.
- (35) Fuchs, O.; Maier, F.; Weinhardt, L.; Weigand, M.; Blum, M.; Zharnikovc, M.; Denlinger, J.; Grunze, M.; Heske, C.; Umbach, E. A liquid flow cell to study the electronic structure of liquids with soft X-rays. *Nucl. Instrum. Methods Phys. Res., Sect. A* **2008**, 585 (3), 172–177.
- (36) Hedman, J.; Heden, P. F.; Nordling, C.; Siegbahn, K. Energy Splitting of Core Electron Levels in Paramagnetic Molecules. *Phys. Lett.* A **1969**, 29 (4), 178–179.
- (37) Avval, T. G.; Chatterjee, S.; Hodges, G. T.; Bahr, S.; Dietrich, P.; Meyer, M.; Thissen, A.; Linford, M. R. Oxygen gas, O-₂(g), by near-ambient pressure XPS. *Surf. Sci. Spectra* **2019**, *26* (1), 014021.
- (38) Zaera, F. Probing Liquid/Solid Interfaces at the Molecular Level. *Chem. Rev.* **2012**, *112* (5), 2920–2986.
- (39) Zaera, F. New advances in the use of infrared absorption spectroscopy for the characterization of heterogeneous catalytic reactions. *Chem. Soc. Rev.* **2014**, 43 (22), 7624–7663.
- (40) Campion, A.; Kambhampati, P. Surface-enhanced Raman scattering. Chem. Soc. Rev. 1998, 27 (4), 241–250.
- (41) Shen, Y. R.; Ostroverkhov, V. Sum-frequency vibrational spectroscopy on water interfaces: Polar orientation of water molecules at interfaces. *Chem. Rev.* **2006**, *106* (4), 1140–1154.
- (42) Bechtel, H. A.; Muller, E. A.; Olmon, R. L.; Martin, M. C.; Raschke, M. B. Ultrabroadband infrared nanospectroscopic imaging. *Proc. Natl. Acad. Sci. U. S. A.* **2014**, *111* (20), 7191–7196.
- (43) Centrone, A. Infrared Imaging and Spectroscopy Beyond the Diffraction Limit. *Annu. Rev. Anal. Chem.* **2015**, *8*, 101–126.

- (44) Muller, E. A.; Pollard, B.; Bechtel, H. A.; van Blerkom, P.; Raschke, M. B. Infrared vibrational nano-crystallography and nano-imaging. *Sci. Adv.* **2016**, *2* (10), e1601006.
- (45) Baskin, A.; Prendergast, D. Ion Solvation Spectra": Free Energy Analysis of Solvation Structures of Multivalent Cations in Aprotic Solvents. *J. Phys. Chem. Lett.* **2019**, *10* (17), 4920–4928.
- (46) Baskin, A.; Prendergast, D. Exploring chemical speciation at electrified interfaces using detailed continuum models. *J. Chem. Phys.* **2019**, *150* (4), 041725.
- (47) Huth, F.; Govyadinov, A.; Amarie, S.; Nuansing, W.; Keilmann, F.; Hilenbrand, R. Nano-FTIR Absorption Spectroscopy of Molecular Fingerprints at 20 nm Spatial Resolution. *Nano Lett.* **2012**, *12* (8), 3973–3978.
- (48) Oviroh, P. O.; Akbarzadeh, R.; Pan, D. Q.; Coetzee, R. A. M.; Jen, T. C. New development of atomic layer deposition: processes, methods and applications. *Sci. Technol. Adv. Mater.* **2019**, *20* (1), 465–496.
- (49) Hao, W.; Marichy, C.; Journet, C. Atomic layer deposition of stable 2D materials. 2D Mater. 2019, 6 (1), 012001.
- (50) Akahane, Y.; Asano, T.; Song, B. S.; Noda, S. High-Q photonic nanocavity in a two-dimensional photonic crystal. *Nature* **2003**, 425 (6961), 944–947.
- (51) Sader, J. E.; Chon, J. W. M.; Mulvaney, P. Calibration of rectangular atomic force microscope cantilevers. *Rev. Sci. Instrum.* **1999**, 70 (10), 3967–3969.
- (52) Bluhm, H.; Andersson, K.; Araki, T.; Benzerara, K.; Brown, G. E.; Dynes, J. J.; Ghosal, S.; Gilles, M. K.; Hansen, H. C.; Hemminger, J. C.; Hitchcock, A. P.; Ketteler, G.; Kilcoyne, A. L. D.; Kneedler, E.; Lawrence, J. R.; Leppard, G. G.; Majzlan, J.; Mun, B. S.; Myneni, S. C. B.; Nilsson, A.; Ogasawara, H.; Ogletree, D. F.; Pecher, K.; Salmeron, M.; Shuh, D. K.; Tonner, B.; Tyliszczak, T.; Warwick, T.; Yoon, T. H. Soft X-ray microscopy and spectroscopy at the molecular environmental science beamline at the Advanced Light Source. *J. Electron Spectrosc. Relat. Phenom.* **2006**, *150* (2–3), 86–104.